Molecular dynamics simulations of liquid, interface, and ionic solvation of polarizable carbon tetrachloride

Tsun-Mei Chang, Kirk A. Peterson,[a] and Liem X. Dang[b]
Environmental Molecular Sciences Laboratory, Pacific Northwest Laboratory, Richland, Washington 99352

(Received 25 May 1995; accepted 2 August 1995)

In this study, we construct a nonadditive polarizable model potential to describe the intermolecular interactions between carbon tetrachloride, CCl_4, based on classical molecular dynamics techniques. The potential parameters are refined to accurately describe the experimental thermodynamic and structural properties of liquid CCl_4 at 298 K. We then carried out additional liquid CCl_4 simulations at temperatures in the range of 250–323 K to examine the temperature dependence of the thermodynamic properties. The computed liquid densities and the enthalpies of vaporization are in excellent agreement with experimental values. The structures of liquid CCl_4 can be analyzed by examining the radial distribution functions and angular distribution functions. It is found that the liquid CCl_4 forms an interlocking structure and that a local orientational correlation is observed between neighboring CCl_4 molecules. We also investigate the CCl_4 liquid/vapor interface using this potential model. The density profile shows that the interface is not sharp at a microscopic level and has a thickness of roughly 5 Å at 273 K. The results of angular distribution function calculations suggest that CCl_4 molecules do not have a preferred orientation at the interface. The calculated surface tension is 31 ± 2 dyn/cm, in good agreement with the experimental value of 28 dyn/cm. This model potential is also used to examine the interactions between Cs^+ and small $(CCl_4)_n$ $(n=1-6)$ clusters. A tetrahedral configuration is found for the minimum structure of the $Cs^+(CCl_4)_4$ cluster. It is noticed that the polarization energy is the dominant component of the total interaction of these ionic clusters, indicating the importance of including explicitly the polarization in the ionic interactions. In the study of Cs^+ solvation in liquid CCl_4, we observe a well-defined solvation shell around the Cs^+ with a coordination number of six CCl_4 molecules. It is also found that Cs^+ induces a strong local orientational order in liquid CCl_4. Accurate *ab initio* electronic structure calculations were also carried out on the CCl_4 dimer and the $Cs^+(CCl_4)$ cluster to compare to the results from the molecular dynamics simulations.

I. INTRODUCTION

Computer simulations have proven to be useful tools for examining condensed-phased systems including bulk liquids,[1–3] solids,[4,5] liquid/vapor,[6–8] liquid/liquid,[9–11] and liquid/solid[12,13] interfaces. These studies are not only able to characterize the static structures of these systems at a molecular level, but also provide a method to describe dynamical processes such as solvation and ion transport occurring in these media. The accuracy of these simulations depends critically on the potential models describing the interactions of the systems under investigation. A careless choice of the interaction potentials can often lead to misleading conclusions. Thus, it is essential to construct model potentials that can accurately describe the molecular interactions.

In this study, we will focus on developing a new potential model for carbon tetrachloride (CCl_4). CCl_4, being analogous to simple atomic liquids due to its high molecular symmetry, can serve as a simple model system for the understanding of more complex molecular liquids. CCl_4 is also a very important organic solvent, widely used in the processes of synthesis, purification, and cleaning. Moreover, CCl_4 is of great environmental interest. Due to its usage in the processes of treating radioactive materials, it contributes significantly to the problem of nuclear waste remediation. Therefore, much experimental and theoretical work has been devoted to the understanding of its chemical and physical properties,[14–23] and it is of fundamental importance to develop a potential model that can describe the CCl_4 interactions properly, so one can study processes such as ion transport and chemical reactions in this solvent.

There are several available CCl_4 interaction potentials in the literature.[19–23] Based on x-ray diffraction experiments, Narten *et al.* have constructed several Lennard-Jones type potential models for liquid CCl_4.[19] Their studies seemed to suggest that the properties of liquid CCl_4 can be determined mainly by the interactions between chlorine atoms. It is also shown that a local orientational order is exhibited in liquid CCl_4. Lowden and Chandler proposed a five-site fused hard sphere model for CCl_4.[20] Their structural results, obtained by solving the RISM (reference interaction site model) integral equations, are in satisfactory agreement with the neutron scattering experiments. They found an interlocking structure for liquid CCl_4 and argued that there is a preferred local orientational order between CCl_4 molecules. Later, using molecular dynamics (MD) techniques, McDonald and co-workers[21] constructed a five-site CCl_4 potential model with both Lennard-Jones and Coulombic interaction terms to model the liquid and the plastic crystal states of CCl_4. Their simulations reproduced reasonably well many structural and thermodynamic properties of liquid CCl_4. However, they

[a]Permanent address: Department of Chemistry, Washington State University.
[b]Author to whom all correspondence should be addressed.

 0021-9606/95/103(17)/7502/12/$6.00

predicted a local orientational correlation different from that of Lowden and Chandler.[20] In a Monte Carlo study conducted by Adan *et al.*,[23] a different five-site Lennard-Jones potential has been proposed for CCl_4, which gives liquid CCl_4 structures consistent with experimental results. In this paper, they discussed some limitations for using simple interaction models and addressed the importance of the choice of the asymmetrical C–Cl potential parameters. More recently, Duffy and co-workers[24] as well as DeBolt and Kollman[22] have developed new sets of CCl_4 potential parameters in their studies of solvent effects.

Although there are several available CCl_4 interaction potentials that are able to reproduce reasonably well the thermodynamic and structural properties of CCl_4, these potentials are all pairwise additive in nature and neglect the important ingredient of many-body interactions.[1,25,26] It is well established that nonadditive interactions can make significant contributions to the total interaction energy, and the incorporation of many-body interactions is expected to be especially critical for the study of ionic and interface systems. Although CCl_4 is a nonpolar solvent, it has a very high molecular polarizability. This leads us to suspect that in order to accurately describe CCl_4 molecular interactions, the nonadditive polarizability has to be included explicitly. In the study of solvatochromism by DeBolt and Kollman,[22] they found that a pairwise additive potential was not sufficient to reproduce the spectral shift of the electronic transition of carbonyl compounds in liquid CCl_4. They attributed this deficiency mostly to the lack of nonadditive effects in their interaction potentials.

In the present study, we will focus on constructing a nonadditive polarizable CCl_4 interaction potential. Ideally, the development of such an interaction model would be based on an accurate *ab initio* derived potential energy surface. However, in order to properly describe the polarization effect of CCl_4, large basis sets and high level theories are required. This approach is too computationally intensive to be undertaken at the present time. Therefore, we will use classical molecular dynamics simulations to optimize the potential parameters by fitting the computed thermodynamic, structural, and dynamical properties to the available experimental results. This potential is then applied to model the CCl_4 liquid/vapor interface, and comparison between experimental and computed properties of the liquid/vapor interface is made to assure the validity of the potential. Finally, the potential is employed to examine the solvation properties of a single Cs^+ cation in small $(CCl_4)_n$ $(n=1-6)$ clusters and in bulk liquid CCl_4.

The paper is organized as follows. In Sec. II, we briefly describe the polarizable potential model used in this study. The computational details of the MD simulations are summarized in Sec. III. Properties of the bulk liquid CCl_4 are presented and discussed in Sec. IV. Comparisons of these computed properties to those of the experimental and previous theoretical work are also made. The simulation results of the CCl_4 liquid/vapor interface are summarized in Sec. V. In Secs. VI and VII, we report the solvation properties of the Cs^+ ion in small CCl_4 clusters and in liquid CCl_4. The conclusions are presented in Sec. VIII.

II. POTENTIAL MODEL

In the following, we consider a rigid five-site interaction model potential for carbon tetrachloride. The single CCl_4 is fixed at its experimental tetrahedral geometry[27] with a C–Cl bond length of 1.77 Å and a Cl–C–Cl bond angle of 109.47°. As in the usual pairwise potentials, there are fixed atomic charges and Lennard-Jones potential parameters associated with each atomic site. In addition, there are point polarizabilities assigned to each atom to account for the nonadditive polarization energy. The total interaction energy can be written as

$$U_{\mathrm{tot}} = U_{\mathrm{pair}} + U_{\mathrm{pol}}, \tag{1}$$

where the pairwise additive part of the potential is the sum of the Lennard-Jones and Coulomb interactions,

$$U_{\mathrm{pair}} = \sum_i \sum_j \left(4\epsilon \left[\left(\frac{\sigma_{ij}}{r_{ij}} \right)^{12} - \left(\frac{\sigma_{ij}}{r_{ij}} \right)^{6} \right] + \frac{q_i q_j}{r_{ij}} \right). \tag{2}$$

Here, r_{ij} is the distance between atom site i and j, q is the atom charge, and σ and ϵ are the Lennard-Jones parameters. The nonadditive polarization energy is given by[25]

$$U_{\mathrm{pol}} = -\frac{1}{2} \sum_i \boldsymbol{\mu}_i \cdot \mathbf{E}_i^0, \tag{3}$$

where E_i^0 is the electric field at site i produced by the fixed charges in the system,

$$\mathbf{E}_i^0 = \sum_{j \neq i} \frac{q_j \mathbf{r}_{ij}}{r_{ij}^3}. \tag{4}$$

μ_i is the induced dipole moment at atom site i, and is defined as

$$\boldsymbol{\mu}_i = \alpha \mathbf{E}_i, \tag{5}$$

where

$$\mathbf{E}_i = \mathbf{E}_i^0 + \sum_{j \neq i} \mathbf{T}_{ij} \mu_j. \tag{6}$$

In the above, E_i is the total electric field at atom i, α is the point polarizability, and $\mathbf{T}_{ij}$ is the dipole tensor

$$\mathbf{T}_{ij} = \frac{1}{r_{ij}^3} \left(\frac{3 \mathbf{r}_{ij} \mathbf{r}_{ij}}{r_{ij}^2} - 1 \right). \tag{7}$$

During the molecular dynamics simulations, an iterative procedure is used to solve Eq. (5). The convergence is achieved when the deviations of the dipole moment from two sequential iterations fall to within 0.01 D.

III. SIMULATION DETAILS

In constructing the nonadditive CCl_4 interaction potentials, classical molecular dynamics simulation techniques and *ab initio* calculations are used. The partial charges associated with the carbon and chlorine atoms are determined via quantum electronic structure calculations. Using the GAUSSIAN 92 program,[28] we performed a Hartree–Fock geometry optimization for CCl_4 with the 6-31+G* basis set. The atom-centered point charges were determined via fits to the electrostatic potentials obtained from the calculated CCl_4 wave

TABLE I. Potential parameters for CCl_4 and Cs^+ used in the MD simulations. σ and ϵ are the Lennard-Jones parameters, q is the atomic charge, and α is the atomic polarizability.

Atom type	σ (Å)	ϵ (kcal/mol)	$q(e)$	α (Å^3)
C	3.41	0.10	−0.1616	0.878[a]
Cl	3.45	0.26	0.0404	1.910[a]
Cs^+	3.831[b]	0.10[b]	1.0000[b]	2.440[b]

[a]Reference 29.
[b]Reference 45.

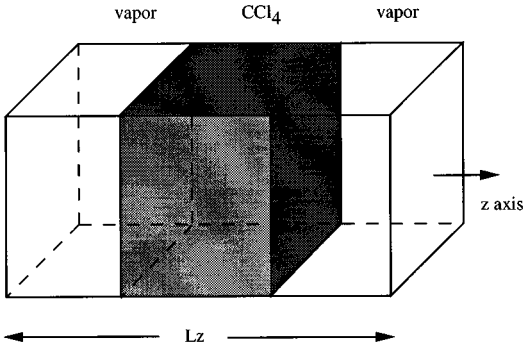

FIG. 1. A schematic representation of the simulation box for the CCl_4 liquid/vapor interface. The liquid phase of CCl_4 is in the middle of the box. The z axis is chosen to be perpendicular to the interface.

functions. Neither the inclusion of correlation nor extensions of the basis set led to appreciable differences in these values. The atomic site polarizabilities for carbon and chlorine are taken from the work of Applequist *et al.*,[29] which reproduced the experimental CCl_4 molecular polarizability to within 1%.[30] Thus only the four Lennard-Jones parameters (σ_{CC}, ϵ_{CC}, σ_{ClCl}, and ϵ_{ClCl}) remain to be determined, with the assumption that the cross interactions between C and Cl and between the ion and C and Cl follow the Lorentz-Berthelot combining rules[2] with

$$\sigma_{kl}=\left(\frac{\sigma_{kk}+\sigma_{ll}}{2}\right) \tag{8}$$

and

$$\epsilon_{kl}=(\epsilon_{kk}\epsilon_{ll})^{1/2}. \tag{9}$$

To optimize these Lennard-Jones parameters, we carried out a series of classical molecular dynamics simulations of liquid CCl_4 at 298 K. During the parameter optimizations, we calculate the structural and thermodynamic properties of bulk CCl_4 including radial distribution functions, densities, and enthalpies of vaporization and compare to experiments. The final potential parameters are obtained when the potential model adequately reproduces the experimental properties of liquid CCl_4. In Table I, the optimized potential parameters are presented.

The actual MD simulations for bulk liquid CCl_4 consist of 265 CCl_4 molecules in a cubic simulation cell with a linear dimension roughly equal to 35 Å. Periodic boundary conditions are applied in all three directions. The simulations are carried out in an isobaric–isothermal (NPT) ensemble at 1 atm and at several temperatures: 250, 273, 298, 313 and 328 K, with time steps for heat bath coupling and pressure relaxation of 0.1 and 0.2 ps, respectively.[31] The initial velocities assigned for each atom are chosen from a Maxwell–Boltzmann distribution corresponding to the desired simulation temperature. The SHAKE algorithm[31] is used during the entire simulation to constrain all the bond lengths in order to fix the CCl_4 internal geometry. In all MD simulations, a time step of 2 fs is used. A potential cutoff of 15 Å is chosen to reduce computational effort. The long-range correction for Lennard-Jones interactions, E_{corr}, is estimated by assuming uniform radial distribution functions (RDFs) after potential cutoff[32]

$$E_{corr}=\frac{N\rho}{2}\int_{r_c}^{\infty}u(r)4\pi r^2 dr. \tag{10}$$

Here, N is the number of molecules in the system, ρ is the density, r_c is the potential cutoff, and $u(r)$ is the intermolecular Lennard-Jones interactions. Since the electrostatic interaction only makes a small contribution to the total potential energy, no long-range correction is considered. At all temperatures, 100 ps trajectories are carried out to equilibrate the system, followed by at least 200 ps of data collection for analysis.

In order to further test the validity of this CCl_4 model potential, additional simulations are carried out to study the CCl_4 liquid/vapor interface. Initially, we took a box of 265 CCl_4 molecules that had been equilibrated for 100 ps at 273 K from previous bulk CCl_4 simulations, and put it into the middle of a simulation cell whose linear dimensions are $34.89\times34.89\times84.89$ Å (see Fig. 1). This creates two CCl_4 liquid–vapor interfaces that are chosen to be perpendicular to the z axis. The whole system is then equilibrated for 100 ps at a constant volume and temperature (NVT ensemble) with periodic boundary conditions applied in all three directions. The interactions are truncated at a molecular center-of-mass separation of 15 Å. The data collected for later analysis are obtained from a 200 ps MD trajectory after initial equilibration.

We also carried out MD simulations to study the solvation properties of Cs^+ interacting with small CCl_4 clusters and in bulk liquid CCl_4. For ion–cluster simulations, the steepest descent and simulated annealing methods are used to obtain the minimal energy structures at 0 K and classical molecular dynamics simulations in an NVE ensemble are carried out to determine the binding enthalpies at higher temperatures. The ionic solution simulation involves a single Cs^+ and 265 CCl_4 molecules embedded in a cubic simulation box of roughly 35 Å. The entire simulation is carried out at a constant pressure of 1 atm and a temperature of 298 K (NPT ensemble) with temperature and pressure coupling constants of 0.1 and 0.2 ps, respectively. Periodic boundary conditions are employed, and a time step of 2 fs is used in solving the equations of motion. As in the bulk CCl_4 simulations, the SHAKE procedure is adopted to fix all bond lengths at their equilibrium value. The nonbonded interactions are truncated at a molecular separation of 15 Å. The statistical analysis is performed from data collected over 280 ps, following a 100 ps simulation of equilibration.

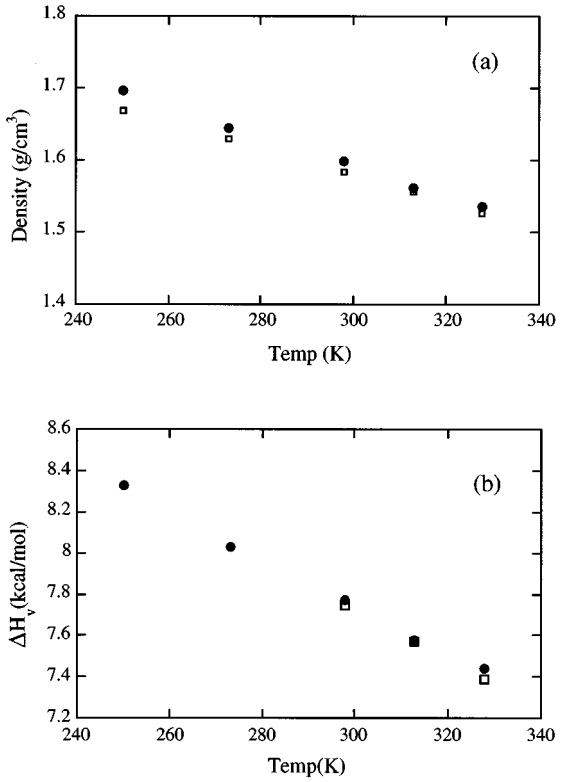

FIG. 2. Temperature dependence of the thermodynamics properties of liquid CCl_4. (a) Comparison of the calculated (filled circles) and the experimental (squares) liquid densities as a function of temperature. (b) Comparison of the calculated (filled circles) and the experimental (squares) enthalpies of vaporization as a function of temperature.

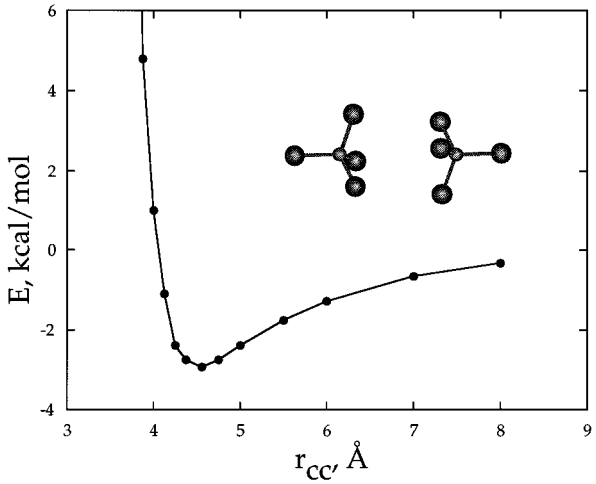

FIG. 3. The gas phase interaction energy for the CCl_4 dimer as a function of the C–C separation. The inset displays the minimum energy structure of the CCl_4 dimer.

IV. LIQUID CCl_4 PROPERTIES

A. Temperature dependence of thermodynamic properties

As mentioned in Sec. III, the potential parameters are optimized by fitting the computed properties to the experimental values at a temperature of 298 K. We feel that this model potential is not only valid at this specific temperature, but is also sufficient for a reasonable temperature range. Thus, we performed a series of computer simulations of bulk CCl_4 liquid at temperatures of 250, 273, 313, and 328 K. The predicted temperature dependence of selected thermodynamic properties is shown in Fig. 2. The computed liquid densities as a function of temperature are depicted in Fig. 2(a), along with the experimental liquid densities. It is clear from Fig. 2 that the calculated densities are in good agreement with the experimental results with the largest deviation of 3% for the entire temperature range. From the computer simulations, one can also calculate the enthalpy of vaporization, $\Delta H_{\mathrm{vap}}(T)$, based on the following relationship:[33]

$$\Delta H_{\mathrm{vap}}(T) = -E_{\mathrm{pot}}(T) - E_{\mathrm{corr}}(T) + RT, \tag{11}$$

where $E_{\mathrm{pot}}(T)$ is the total intermolecular potential energy of liquid CCl_4 at temperature T. Figure 2(b) displays the computed enthalpies of vaporization of liquid CCl_4, which are within 1% of experimental values[16] as clearly demonstrated in Fig. 2. The results from Fig. 2 suggest that although the CCl_4 interaction potential is developed at 298 K, it is also valid for a temperature range of 250–328 K. We have examined various energy components and found that the polarization energy is small compared to other nonbonded interactions. It is thus expected that the effective two-body potential may reproduce many properties of bulk liquid CCl_4. However, we are not only interested in the bulk CCl_4, but also in the processes occurring in CCl_4. It is our goal to develop a model potential that can account for CCl_4 interactions in many different environments. In order to achieve this end, it is necessary to take into account the polarizable component of the CCl_4 interactions. For example, it is suggested that in order to accurately describe the spectral shift of the carbonyl group in CCl_4, the inclusion of polarization is essential.

Although the potential parameters are derived for bulk liquid CCl_4, we also feel it is important to examine the gas phase properties of the CCl_4 dimer. In Fig. 3, we present the optimal configuration and the gas phase interaction energy as a function of the C–C separation for the CCl_4 dimer. We found that the CCl_4 molecules are oriented in such a way as to minimize the repulsive Cl–Cl interactions. The minimum interaction energy for the dimer is about -2.9 kcal/mol with a C–C separation of 4.60 Å. These are in reasonable accord with the results of our MP2/aug-cc-pVDZ calculations, which yield a counterpoise (CP)-corrected binding energy of -3.3 kcal/mol (uncorrected value of 4.17 kcal/mol) and a C–C equilibrium distance of 4.63 Å. Zero-point vibrational corrections, which have not been included for this species, are expected to further decrease this computed binding energy by at least 0.4–0.5 kcal/mol.

B. Structural properties of liquid CCl_4

The structure of liquid CCl_4 can be characterized in terms of the atomic radial distribution functions, $g_{ab}(r)$, which give the probabilities of finding an atom of type b at a distance r away from a center atom of type a. In Figs. 4(a)–4(c), we show the computed C–C, C–Cl, and Cl–Cl radial distribution functions as a function of temperature. In general, the features of these atomic radial distribution func-

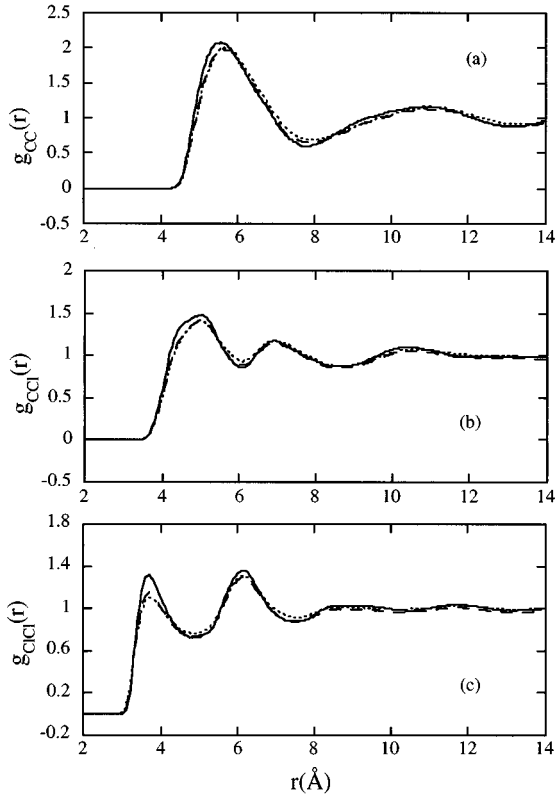

FIG. 4. The atomic radial distribution functions as a function of temperature from bulk CCl_4 simulations. Plots (a)–(c) correspond to the C–C, C–Cl, and Cl–Cl radial distribution functions respectively, for $T=250$ (solid line), 298 (dashed line), and 323 K (dotted line).

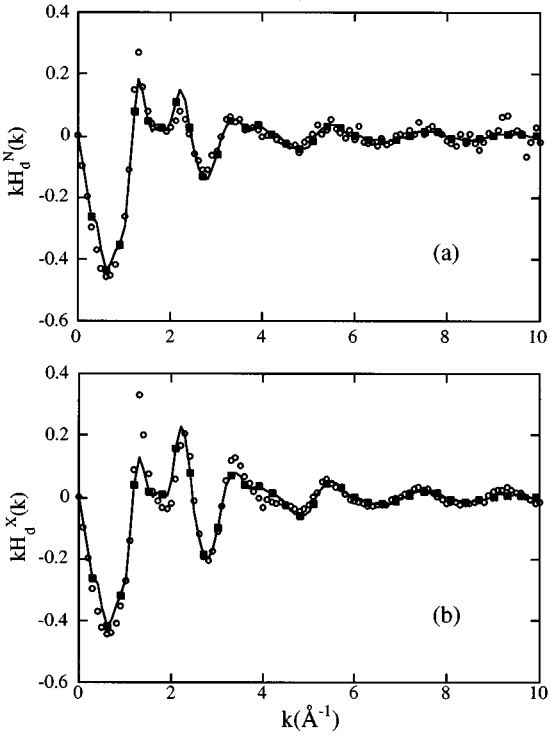

FIG. 5. The functions $kH_d^N(k)$ [shown in (a)] and $kH_d^X(k)$ [shown in (b)] for liquid CCl_4. The solid line with filled squares is from the MD simulation at 298 K and the experimental results (circles) were obtained by Narten at 293 K.

tions, respectively, are consistent with those reported in the literature with different CCl_4 interaction potentials. By examining these figures, it is found that the overall shape of the radial distribution functions remain the same for all temperatures, suggesting that not many structural changes occur. As the temperature increases, the peak positions of the RDFs shift toward larger distances, correlating with decreasing liquid densities at higher temperatures. Note that at the same time, the amplitudes of the peaks in the radial distribution functions are somewhat broadened due to larger thermal fluctuations at higher temperatures. Integrating over the first peak of $g_{CC}(r)$ gives about 12 neighboring carbon atoms in the first coordination shell of a central carbon atom. This observation implies that liquid CCl_4 resembles a closed-packed, monatomic liquid, as suggested in previous studies.[21,34] It is also clear from Fig. 4(a) that there is a long-range oscillation located well beyond 14 Å for $g_{CC}(r)$. Compared to those of $g_{CC}(r)$, the correlations of $g_{CCl}(r)$ and $g_{ClCl}(r)$ have a much shorter range. The first two peak positions of $g_{CCl}(r)$ and $g_{ClCl}(r)$ are in excellent agreement with the experimentally deduced values of 4.9 and 7.2 Å for $g_{CCl}(r)$, and of 3.8 and 6.2 Å for $g_{ClCl}(r)$.[34]

In order to compare directly to the results from neutron scattering and x-ray experiments, we Fourier transform the radial distribution functions into atomic partial structure factors, $S_{ab}(k)$, according to[2]

$$S_{ab}(k)=4\pi\rho\int_0^\infty |g_{ab}(r)-1|\,\frac{\sin kr}{kr}\,r^2dr, \tag{12}$$

where r is the liquid density. The signal intensities in the x-ray and neutron scattering experiments, $H_d^N(k)$ and $H_d^X(k)$, as a function of the wave vector k, are simply weighted combinations of the partial structure factors[21,23]

$$H_d^N(k)=0.02S_{CC}(k)+0.25S_{CCl}(k)+0.73S_{ClCl}(k), \tag{13}$$

$$H_d^X(k)=0.00S_{CC}(k)+0.12S_{CCl}(k)+0.88S_{ClCl}(k). \tag{14}$$

We show in Figs. 5(a) and 5(b) the computed $kH_d^N(k)$ and $kH_d^X(k)$ for liquid CCl_4 at 298 K, along with the experimental curves obtained by Narten at 293 K.[34] The agreement between the simulations and experiments is, in general, satisfactory. The discrepancy between experiment and our calculations at small k is most likely due to the finite size of the simulations, since it is well known that long-range oscillations of $g(r)$ dominate the behavior of $S(k)$ at small k.

There is an unresolved issue in the literature concerning the local orientational structure between CCl_4 molecules. Lowden and Chandler,[20] Egelstaff *et al.*,[35] and McDonald and co-workers[21] have all proposed different configurations for the preferred orientation between CCl_4 molecules (see Fig. 1 in Ref. 21). The disagreement can be explained by examining the probability distribution of the angle between the intramolecular C–Cl bond and the vector connecting the carbon atom to another carbon atom. Figure 6 depicts such angular distribution functions, $P(\theta,r)$, as a function of the

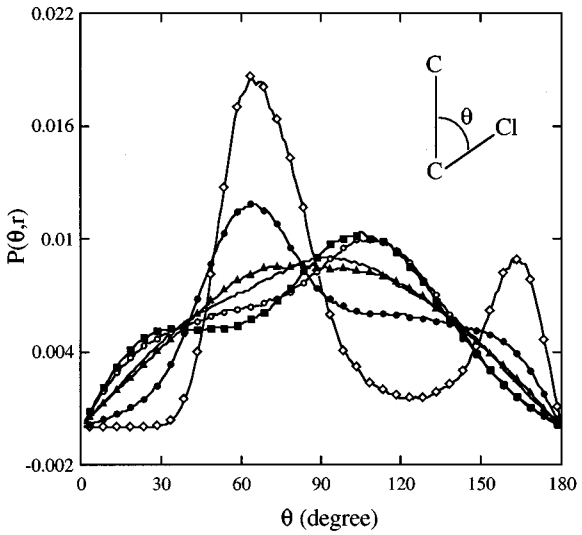

FIG. 6. The probability distributions for an angle between the intramolecular C–Cl bond and the vector connecting two C's as a function of the C–C distance. The symbols correspond to C–C distances of 0–5 (diamonds), 5–6 (dark circles), 6–7 (circles), 7–8 (dark squares), and 8–9 Å (filled triangles). The solid curve is the sine function that describes a uniform angular distribution.

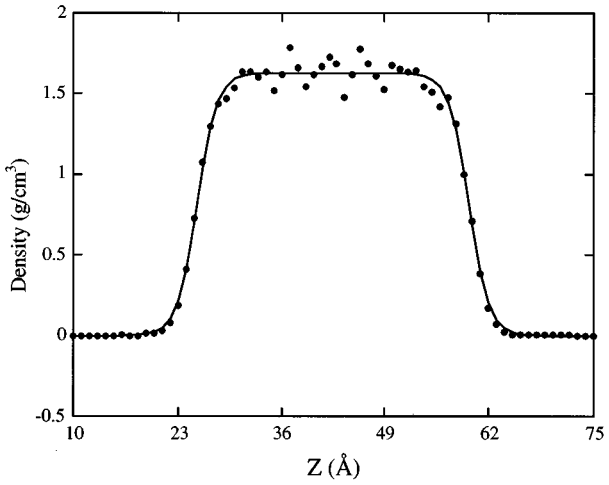

FIG. 7. The computed density profile (filled circles) from the CCl_4 liquid/vapor interface simulation at 273 K. The solid line is the best fit to Eq. (17).

C–C distance. Due to the broad features of the angular distribution functions, it is implausible to consider only one type of configuration dominating the local orientation. However, it is clear that when the C–C distance is less than 5 Å, the interlocking configuration suggested by Lowden and Chandler[20] is the most important as indicated by the peaks at 67° and 163° in the angular distribution functions, in contrast to the prediction of McDonald *et al.*[21] based on energic arguments. When the C–C distance increases to about the first peak position in the $g_{CC}(r)$, other configurations start to show significant contributions while the interlocking structure remains important. As the C–C distance increases, the angular distribution functions approach the sine function that describes a uniform orientation, indicating the vanishing of an orientational correlation.

C. Dynamical properties

We can calculate the self-diffusion coefficient of liquid CCl_4 by monitoring the mean square displacement, $\langle r^2(t)\rangle$, as a function of time

$$\langle r^2(t)\rangle = \frac{1}{N}\sum_i |r_i(t) - r_i(0)|^2, \tag{15}$$

where $r_i(t)$ is the position of molecule i at time t, and N is the number of molecules in the system. We have calculated the mean square displacement from the MD simulation at 298 K in a NVT ensemble, which forms a straight line as a function of time (data not shown). The diffusion constant can be deduced from these results by taking the limiting value of the slope

$$D = \lim_{t\to\infty} \frac{\langle r^2(t)\rangle}{6t}. \tag{16}$$

This leads to a diffusion constant of $(1.8\pm0.2)\times10^{-5}$ cm^2/s, in reasonable agreement with the experimental result of 1.3×10^{-5} cm^2/s at 293 K.[14]

Comparing the computed thermodynamic, structural, and dynamical properties from MD simulations to those of the experiments suggests that the present CCl_4 model potential gives a good description of the CCl_4 interactions in bulk liquid.

V. CCl_4 LIQUID/VAPOR INTERFACE

A. Density profile

In Fig. 7, we present the computed CCl_4 density profile as a function of the z coordinate from CCl_4 liquid/vapor simulations at 273 K. As clearly indicated in Fig. 7, two well-defined stable interfaces exist, which are symmetric around the center of mass of the whole system. There is a region of bulklike CCl_4 having a size of 30 Å between these two interfaces with a liquid density of 1.63 g/cm^3, which is very close to the bulk density at 273 K. The density profile can be fit by a hyperbolic tangent functional form[8,36]

$$\rho(z) = \tfrac{1}{2}(\rho_L+\rho_V) - \tfrac{1}{2}(\rho_L-\rho_V)\tanh[(z-z_0)/d], \tag{17}$$

where ρ_L and ρ_V are the liquid and vapor densities, respectively, z_0 is the position of the Gibb's dividing surface, and d estimates the thickness of the interface. The best-fit curve is also shown in Fig. 7. An estimate of the interfacial width of 5.0 Å is obtained from this fit. This indicates that the liquid–vapor interface is not microscopically smooth. The so-called "10–90" thickness, t, of a hyperbolic tangent is related to d by $t=2.197d$, yielding a value of t of 11.0 Å. Interestingly, by examining Fig. 7 more closely, we find that there seems to be oscillations of the density profile. There is a long-existing debate over the reality of this oscillatory behavior.[37] Recently, Evans and co-workers predicted that the oscillation of the density profile is closely related to the spatial correlation of the molecular radial distribution functions based on density functional theory.[38] Due to the long-range correlation of $g_{CC}(r)$, we would have to use much larger simulation sys-

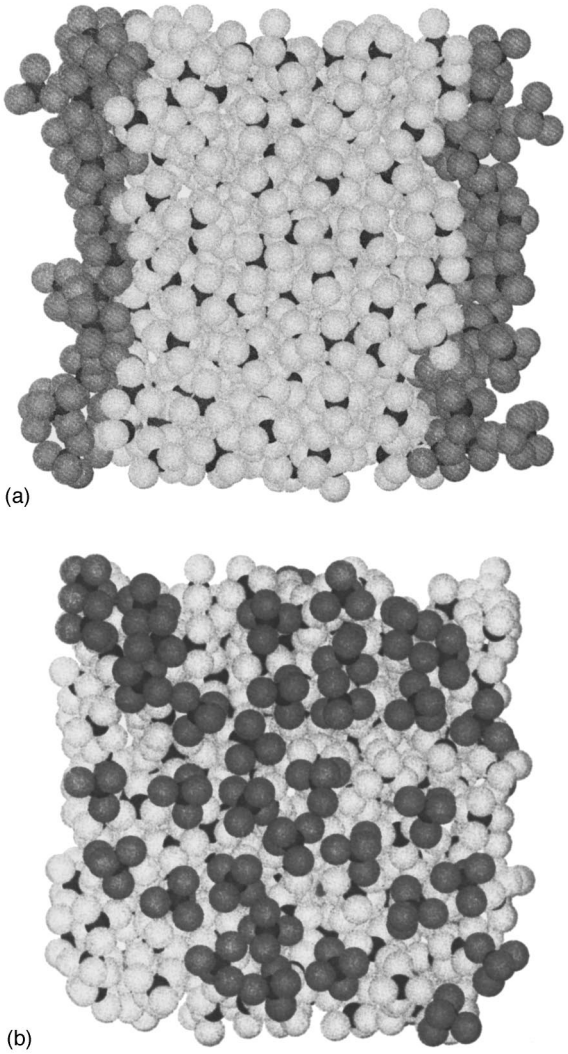

FIG. 8. Snapshots of the instantaneous structure of the CCl_4 liquid/vapor interface. The dark color corresponds to carbon atoms and chlorine atoms at the surface, and the light color corresponds to chlorine atoms in the bulk plots (a) and (b) show typical structures of the side and the top of the interface, respectively.

tems in order to resolve this point, which is not the main concern in this study. However, it will be interesting in the future to perform a systematic study on liquid/vapor interfaces to investigate the oscillatory nature of the density profile. In Fig. 8, we show snapshots taken from the top and the side of the CCl_4 liquid/vapor interface. Obviously, there are thermal fluctuations in the interface positions and the surface is not sharp at a molecular level. A summary of the thermodynamic properties of polarizable CCl_4 is presented in Table II. It is clear that the present model gives a good description of the CCl_4 interactions both in the bulk and at the liquid/vapor interface.

TABLE II. Thermodynamic properties for polarizable CCl_4 at 298 K and 1 atm.

	This work	Experiment
ρ, g/cm^3	1.59±0.02	1.58
ΔH_{vap}, kcal/mol	7.77±0.07[a]	7.74
Surface tension, dyn/cm	31±2	28[b]
Diffusion, 10^{-5} cm^2/s	1.8±0.2	1.3[c]
Dimer energy, kcal/mol	−2.9	
C–C dimer distance, Å	4.6	

[a]$\Delta H_{vap}=-E_{pot}-E_{corr}+RT$, $E_{pot}=-7.02$ kcal/mol, $E_{corr}=-0.13$ kcal/mol.
[b]Reference 42.
[c]Reference 14.

B. Structure

The structural changes between CCl_4 in the bulk and at the interface can be characterized by the atomic radial distribution functions, $g_{ab}(r,z)$, as a function of the z coordinate of the CCl_4 molecule. Thus, the simulation cell is divided into several slabs along the z direction. For each atom of type a in each slab, the number of atoms of type b that are in a spherical shell of thickness dr that is a distance r away from the central atom a is recorded, regardless of the z position of the b atoms. The z-dependent radial distribution functions are simply defined as the number of neighbors divided by the total number of atoms of type a in the slab and the average number of atoms b inside the spherical cell in the bulk liquid. In other words, we use the bulk radial distribution functions as the references to the z-dependent radial distribution functions. Figures 9(a)–9(c) depict the computed radial distribution functions for C–C, C–Cl, and Cl–Cl as a function of the z coordinate, respectively (where the small z indicates the interfacial region and the large z indicates the bulk region). The peak positions of these radial distribution functions are almost independent of the z coordinates, suggesting that the local structures of CCl_4 remain unchanged from the bulk to the interface. However, we do observe a decrease in the peak height of the radial distribution functions as the CCl_4 approaches the surface. This is entirely due to the departure of CCl_4 molecules into the vapor side of the interface. In principle, the magnitude of the molecular radial distribution functions at the interface should be half that of the bulk radial distribution functions for a planar interface. This is demonstrated by the $g_{ab}(r,z)$ centered around the Gibb's dividing surface at $z=26$ Å.

It is well known that for molecules with directional interactions, the interface may induce an orientational order at the liquid/vapor surface,[35] as observed in the case of the H_2O liquid/vapor interface.[7,34] For the case of CCl_4, due to the high molecular symmetry, we expect to see little, if any, orientational order at the interface. By examining the probability distributions for the angle between the intramolecular C–Cl bond and the interfacial normal direction (z axis) as a function of z in Fig. 10, we found that the data points all fall on the sine curve that describes a uniform distribution of angular distribution regardless of the z coordinate. These results suggest that CCl_4 does not have a preferred orientational order at the interface, as expected.

C. Surface tension

To further test the present interaction model, we calculate the surface tension, γ, which is defined as the difference between the pressure components in the direction parallel and perpendicular to the interface[8,11,39–41]

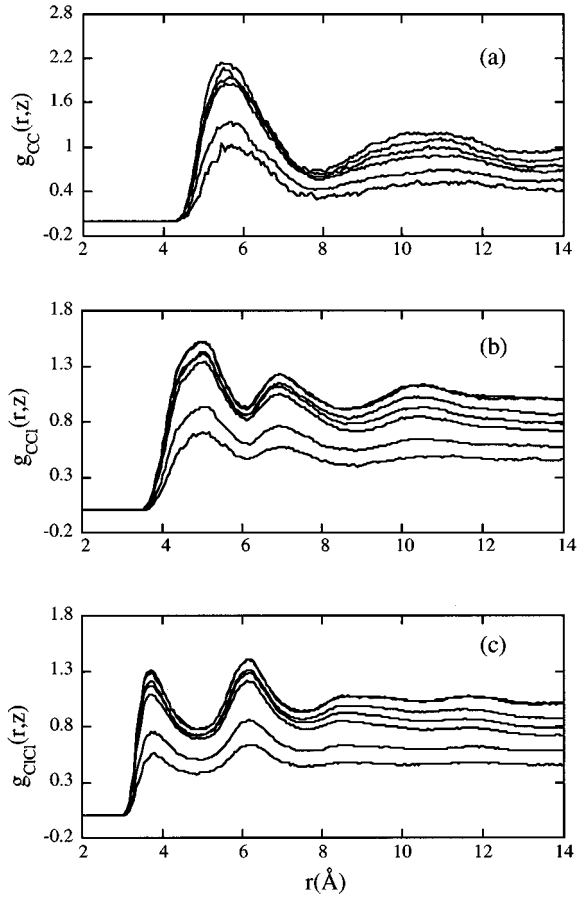

FIG. 9. The atomic radial distribution functions as a function of the z coordinate of the liquid slabs from the CCl_4 liquid/vapor simulations. In (a)–(c), we present the computed C–C, C–Cl, and Cl–Cl radial distribution functions, respectively. The solid curves from the top to the bottom correspond to the liquid slab centered at $z=39$, 36, 33, 20, 27, and 24 Å, respectively.

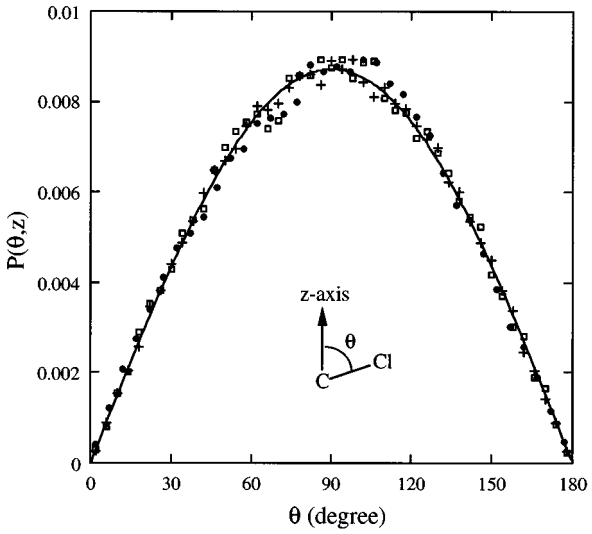

FIG. 10. Probability distributions for the angle between the z axis and the intramolecular C–Cl bond. The data points correspond to the liquid slab centered at $z=24$ (squares), 27 (dark circles), and 30 Å (crosses). The solid curve is the sine function that describes a uniform angular distribution.

$$\gamma=\frac{1}{2}\left(\frac{p_{xx}+p_{yy}}{2}-p_{zz}\right)L_z. \tag{18}$$

In the above, $p_{\alpha\alpha}$ ($\alpha=x$, y, or z) is the $\alpha\alpha$ element of the pressure tensor and L_z is the linear dimension of the simulation cell in the z direction. According to the virial equation, the ab element of the pressure tensor is

$$p_{\alpha\beta}=\frac{1}{V}\left(\sum_{i=1}^{N} m_i v_{i\alpha} v_{i\beta}+\frac{1}{2}\sum_{i'=1}^{N'}\sum_{j'=1}^{N'} F_{i'j'\alpha} r_{ij\beta}\right), \tag{19}$$

where N and N' are the numbers of molecules and atoms, respectively, V is the total volume of the system, m_i is the mass of molecule i, and $v_{i\alpha}$ is the center-of-mass velocity of molecule i. In the above expression, $F_{i'}j'\alpha$ is the α component of the force exerted on atom i' of molecule i due to atom j' of molecule j, and $r_{ij\beta}$ is the β component of the vector connecting the center of mass of molecules i and j. This formula is proven valid only for pairwise additive potentials. Although the polarizable potential is nonadditive in nature, due to the mathematical requirement of a vanishing derivative of the potential with respect to the induced dipole moment at equilibrium,[25] the polarizable potential effectively becomes pairwise additive after Eq. (5) is satisfied. Thus, Eq. (19) should still be applicable in this case. From a 200 ps MD trajectory, the calculated surface tension is 31 ± 2 dyn/cm, in good agreement with the experimental value of 28 dyn/cm.[42]

VI. IONIC CLUSTERS, $Cs^+(CCl_4)_n$ ($n=1-6$)

Considerable theoretical and computational effort has been focused on the study of aqueous solvation; in contrast, relatively little work has been done on nonaqueous solvents, with the exception of the work by Jorgensen, Klein, and co-workers.[43,44] The motivation for our work on ionic solvation in CCl_4 and its derivatives (i.e., $CHCl_3$ and CH_2Cl_2) is to examine the detailed solvation properties of ionic clusters and ionic solutions of CCl_4, and to compare them with the corresponding results obtained for the ion–water clusters and aqueous ionic solution studies.[45] We begin these studies by examining the minimum energy structure of $Cs^+(CCl_4)_n$, the binding enthalpy, as well as the solution properties of the solvated Cs^+. The potential parameters for the Cs^+ cation are taken from our earlier work on the Cs^+ solvation in aqueous solution,[45] and the cross interactions between Cs–C and Cs–Cl are obtained via the Lorentz–Berthelot combining rule. These studies will serve as the basic foundation for our future work on the mechanism of ion transport between the interface (i.e., the water–carbon tetrachloride interface)

We can identify the lowest-energy structures of the ionic clusters $Cs^+(CCl_4)_n$ using combined simulated annealing and the steepest descent methods. The structures are shown in Fig. 11. For the $Cs^+(CCl_4)_2$ ionic cluster, the minimized structure has a triangular geometry. For the $Cs^+(CCl_4)_3$ cluster, the three carbon atoms form an equilateral triangle which the Cs^+ sits above, resulting in a pyramid structure. The minimized structure of $Cs^+(CCl_4)_4$ consists of the four CCl_4 molecules forming a tetrahedron around the Cs^+. Also clearly shown in Fig. 11 is that Cs^+ induces a well-ordered

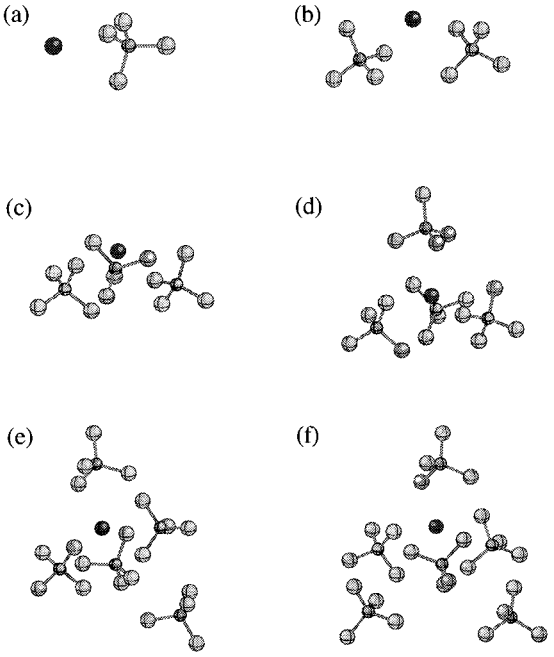

FIG. 11. The lowest-energy structures of ionic clusters at 0 K: (a) Cs^+CCl_4, (b) $Cs^+(CCl_4)_2$, (c) $Cs^+(CCl_4)_3$, (d) $Cs^+(CCl_4)_4$, (e) $Cs^+(CCl_4)_5$, (f) $Cs^+(CCl_4)_6$.

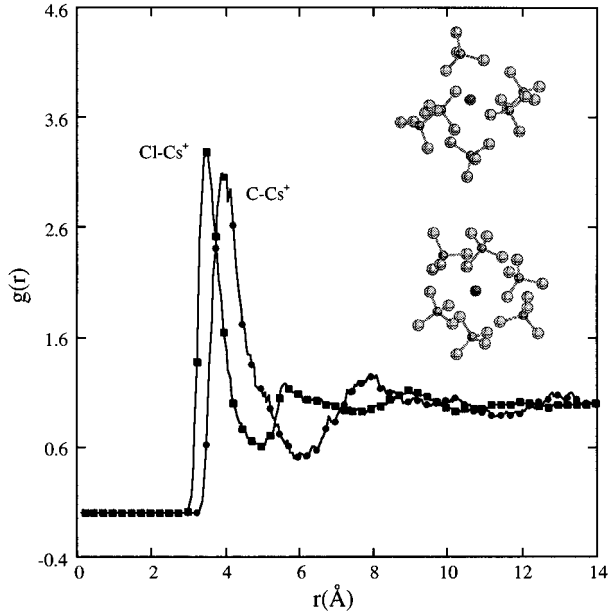

FIG. 12. The computed radial distribution functions for Cs^+–C (solid line with filled circles) and Cs^+–Cl (solid line with filled squares) from the MD simulation of a single Cs^+ in liquid CCl_4 at 298 K. Snapshots of Cs^+ with CCl_4 molecules in the first solvation shell are also shown.

local orientation in the surrounding CCl_4 molecules. Each CCl_4 molecule is found to have three chlorine atoms facing the Cs^+ with almost equal distance. The other chlorine atom is pointing away from Cs^+ with the angle between Cs^+–C and C–Cl being 180°. The minimized structures of $Cs^+(CCl_4)_5$ and $Cs^+(CCl_4)_6$ indicate that the Cs^+ ion is directly coordinated with four CCl_4 molecules in the gas phase and that the additional CCl_4 molecules begin to form a second solvation shell.

We also performed a series of MD simulations on these clusters near 300 K to determine the successive binding enthalpies. The results are given in Table III. To our knowledge, there are no experimental measurements of the successive binding enthalpy for $Cs^+(CCl_4)_n$ clusters. The calculated enthalpy of binding of −7.5 kcal/mol and the average Cs–C distance between 3.8 and 3.9 Å for the $Cs^+(CCl_4)$ are in good agreement with our MP2/aug-cc-pVDZ results of −7.0 kcal/mol (ΔH at 300 K) and 3.95 Å (equilibrium distance), respectively. The *ab initio* enthalpy corrections were obtained from frequencies calculated at the MP2/aug-cc-pVDZ level of theory and were applied to a computed equilibrium binding energy (CP corrected) of −7.24 kcal/mol. (The equilibrium binding energy uncorrected for BSSE was −8.01 kcal/mol.) A complete study of the CCl_4 dimer and $Cs^+(CCl_4)$ interactions via *ab initio* electronic structure calculations will be reported in a forthcoming paper.[46]

TABLE III. Structural and thermodynamic properties of Cs^+ in liquid CCl_4 at 298 K.

	MD simulation
r_{Cs-C} (Å)	3.90
r_{Cs-Cl} (Å)	3.45
Cs–C coordination No.	6.3
ΔH_{sol} (kcal/mol)	−36.5[a]

[a]The solvation energy of Cs^+ in liquid CCl_4 is calculated as the difference between the total potential energy of the Cs^+–CCl_4 system and that of a pure CCl_4 system. We have included the Born correction (−6.1 kcal/mol) for a Cs^+–CCl_4 potential cutoff of 15 Å.

From Table III, we observe that the Cs^+–CCl_4 interactions are significantly smaller than those of the Cs^+–H_2O interactions. This is likely due to a strong ion–dipole interaction in the Cs^+–H_2O system, which is absent in the Cs^+–CCl_4 interaction. If we decompose the Cs^+–CCl_4 interaction into various components, it is found that the polarization energies make the dominant contributions to the total binding energies in these ionic clusters. This indicates that although CCl_4 is a nonpolar molecule, the large polarizability of CCl_4 can play an important role in determining the ion–CCl_4 interactions.

VII. IONIC SOLUTION

We have also examined the solvation properties of the Cs^+ ion in liquid CCl_4. The structure of Cs^+ in CCl_4 can be conveniently described by the ion–CCl_4 radial distribution functions and the angular distribution functions. The dynamical behavior of the Cs^+ ion is characterized by the velocity autocorrelation functions.[47]

A. Structure

The ion–CCl_4 radial distribution functions are displayed in Fig. 12. These radial distribution functions possess well-characterized maxima and minima, indicating the presence of local structural order of CCl_4 around Cs^+. The rather sharp first peak of the $g_{CsC}(r)$ suggests that the CCl_4 molecules form a well-defined solvation shell surrounding Cs^+.

TABLE IV. Calculated average potential energies and the corresponding enthalpies of binding (kcal/mol) of Cs^+–$(CCl_4)_n$ clusters at 300 K using molecular dynamics simulation technique.[a]

n	ΔE	ΔH[b]
1	−6.8±0.5	−7.5±0.5
2	−12.1±1.0	−13.3±1.0
3	−16.6±1.4	−18.4±1.4
4[c]	−23.2±1.4	−25.3±1.4
5[c]	−28.3±1.4	−30.6±1.4
6[c]	−34.2±1.4	−36.6±1.4

[a]The simulations were carried out with a 100 ps equilibration period following 1000 ps for averaging.
[b]$\Delta H=\Delta E-nRT$.
[c]These simulations were carried out at 260, 230, and 200 K for clusters with $n=4$, 5 and 6, respectively, because these clusters evaporate above these temperatures.

Integrating out to the first minimum in $g_{CsC}(r)$ gives a coordination number of six CCl_4 molecules in the first solvation shell of Cs^+, as compared to the coordination of eight water molecules around Cs^+ in the water solutions. The difference comes from the fact that CCl_4 is a much bigger molecule than H_2O; energetically it is unfavorable to pack as many CCl_4 molecules around Cs^+ due to steric effects. Snapshots of the structures of Cs^+ with its first solvation shell of CCl_4 are shown in Fig. 12. The solvation energy of Cs^+ in liquid CCl_4 is calculated as the difference between the total potential energy of the Cs^+–CCl_4 system and that of a pure CCl_4 system. This yields a solvation energy of −36.5 kcal/mol, which is much smaller than the solvation energy of −76.5 kcal/mol for Cs^+ in water. This is partially due to the fact that the Cs^+–H_2O interaction is much stronger than the Cs^+–CCl_4 interaction as mentioned previously, and partially due to the larger coordination number of H_2O with respect to CCl_4 in the first solvation shell of the Cs^+ ion. The solvation properties of Cs^+ in bulk CCl_4 at 298 K are summarized in Table IV.

B. Orientation

The static orientation of CCl_4 molecules surrounding Cs^+ is examined via the angular distribution function as a function of C–Cs^+ distance and is shown in Fig. 13. The angle is defined between the intramolecular C–Cl bond and the vector connecting the Cs^+ and the carbon atom. When the C–Cs^+ distance is smaller than the first peak position of $g_{CsC}(r)$, the computed angular distribution functions show dramatic deviations from the sine curve that describes a uniform distribution. Two peaks centered at 70° and 178° are observed for a C–Cs^+ distance of less than 4 Å, while the probability of finding CCl_4 in another orientation is almost vanished. Integrating over the area under these two peaks gives a ratio of magnitude of roughly 3:1. This implies that each CCl_4 molecule has three of its chlorine atoms facing Cs^+, while the fourth chlorine atom sits on the opposite side of the central carbon atom away from Cs^+ in an almost linear arrangement. The above result suggests that Cs^+ induces a strong local orientational order in liquid CCl_4, which is consistent with the study of the ionic clusters. As the C–Cs^+ distance becomes larger, the angular distribution curve behaves as a normal sine function, indicating that the orientational order has been smeared out.

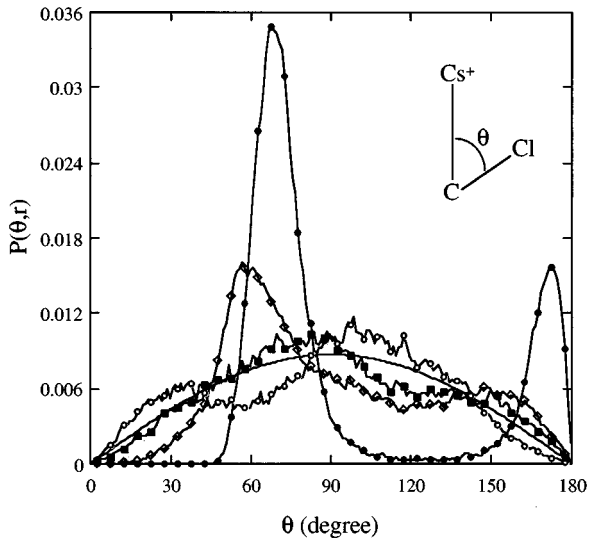

FIG. 13. Probability distributions for the angle between the intramolecular C–Cl bond and the vector pointing from C to the Cs^+ ion as a function of the Cs^+–C distance. The data points correspond to Cs^+–C distances from 0–4 (filled circles), 4–5 (diamonds), 5–6 (circles), and 6–7 Å (filled squares), respectively. Also shown is a sine curve.

C. Dynamical properties

The solvation dynamics of Cs^+ in liquid CCl_4 can be conveniently described in terms of the velocity autocorrelation functions $\hat{C}_{\nu\nu}(t)$, which is defined as[47]

$$\hat{C}_{\nu\nu}(\tau)=\langle V(0)V(\tau)\rangle=\frac{1}{N}\frac{1}{t_{\max}}\sum_{i=1}^{N}\sum_{t=0}^{t_{\max}}V_i(t+\tau)V_i(t). \tag{20}$$

In the above, $V_i(t)$ is the velocity of the ith Cs^+ ion at time t, N is the number of Cs^+ ions in the system, and $t_{\max}$ is the total number of time steps. The velocity autocorrelation function is usually normalized by

$$C_{\nu\nu}(\tau)=\frac{\langle V(0)V(\tau)\rangle}{\langle V(0)V(0)\rangle}. \tag{21}$$

In Fig. 14, we show the normalized velocity autocorrelation function of Cs^+ in liquid CCl_4 as a function of time. The computed curve does not follow a normal exponential decay. The oscillatory behavior of $C_{\nu\nu}(t)$ may come from the motion of Cs^+ inside the first solvation shell of CCl_4. The diffusion constant can be evaluated by integrating the velocity autocorrelation function

$$D=\frac{1}{3}\lim_{t\to\infty}\int_0^t\hat{C}_{\nu\nu}(\tau)d\tau, \tag{22}$$

yielding an estimate of the diffusion constant of 2.6×10^{-5} cm^2/s for Cs^+ in liquid CCl_4 at 298 K.

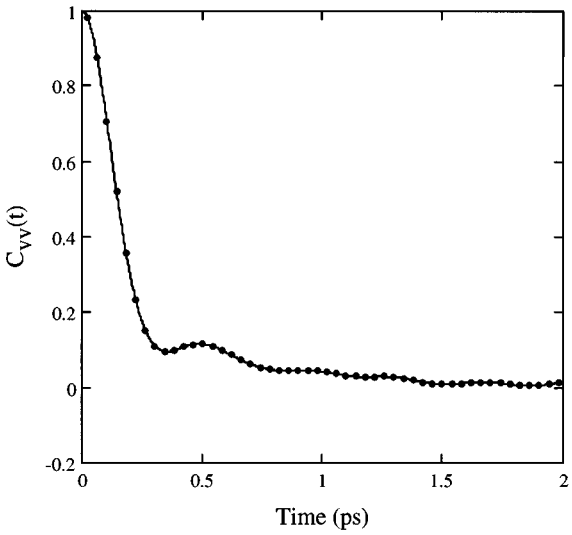

FIG. 14. Normalized velocity autocorrelation functions of Cs^+ in liquid CCl_4 from the MD simulation at 298 K.

VIII. CONCLUSIONS

Using classical molecular dynamics techniques, we have developed a nonadditive polarizable CCl_4 model potential. The computed densities and enthalpies of vaporization from a series of liquid CCl_4 simulations are in excellent agreement with the experimental values for a temperature range of 250–323 K. We characterized the structures of liquid CCl_4 via the atomic radial distribution functions, which also agree reasonably well with experimental measurements. This leads to the conclusion that the present potential model is able to accurately describe the essential elements of the CCl_4 interactions. Liquid CCl_4 is found to form an interlocking structure and exhibit a preferred local orientational correlation between neighboring molecules as proposed in previous studies.[20]

This potential has been employed to examine the CCl_4 liquid/vapor interface. It is observed that the structure of this interface is not smooth at a molecular level and CCl_4 molecules do not have a preferred orientational order at the interface. The agreement between the calculated and experimental surface tensions suggests that the present potential is able to describe CCl_4 molecular interactions in a heterogeneous environment. It is important to point out here that the polarization energy is relatively small for the CCl_4 liquid/vapor interface because CCl_4 is a nonpolar molecule. Therefore, it is anticipated that the effective two-body effective potential may describe this interface reasonably well. However, this is not true for studies of the liquid/liquid interface. For example, in our current study of the liquid CCl_4/H_2O interface,[48] we observe that the induced dipole moments of CCl_4 increase significantly near the interface due to the presence of the polar solvent–H_2O. This effect cannot be described by the effective two-body potentials and demonstrates the importance of including polarization in the CCl_4 potential model.

We have also studied the solvation properties of Cs^+ in small $(CCl_4)_n$ $(n=1-6)$ clusters and in bulk liquid CCl_4. In the case of Cs^+ interacting with small CCl_4 clusters, the polarization energies are found to be the dominant components, indicating the importance of explicitly including the molecular polarizability in modeling the ion–solvent interactions. In bulk liquid CCl_4, Cs^+ is shown to induce a strong local orientational correlation in the surrounding CCl_4 molecules. The atomic radial distributions and the velocity autocorrelation functions suggest that CCl_4 molecules form a well-defined solvation shell around the Cs^+ ion.

ACKNOWLEDGMENTS

This work was performed under the auspices of the Division of Chemical Sciences, Office of Basic Energy Sciences, US Department of Energy under Contract No. DE-AC06-76RLO 1830 with Battelle Memorial Institute, which operates the Pacific Northwest Laboratory, a multiprogram national laboratory. We wish to thank our colleague Dr. Steven Mielke at PNL for his critical reading of the manuscript.

[1] J. Caldwell, L. X. Dang, and P. A. Kollman, J. Am. Chem. Soc. **112**, 9144 (1990).
[2] M. P. Allen and D. J. Tildesley, *Computer Simulation of Liquids* (Oxford University Press, Oxford, 1987).
[3] G. King and A. Warshel, J. Chem. Phys. **93**, 8682 (1990).
[4] P. C. Weakliem and E. A. Carter, J. Chem. Phys. **98**, 737 (1993).
[5] R. M. Lyndenbell, Science **263**, 1704 (1994).
[6] J. K. Lee, J. A. Baker, and G. M. Pound, J. Chem. Phys. **60**, 1976 (1974).
[7] C. A. Croxton, Physica A **106**, 239 (1981).
[8] J. Alejandre, D. J. Tildesley, and G. A. Chapela, J. Chem. Phys. **102**, 4574 (1995).
[9] P. Linse, J. Chem. Phys. **86**, 4177 (1987).
[10] M. Meyer, M. Mareschal, and M. Hayoun, J. Chem. Phys. **89**, 1067 (1988).
[11] A. R. Van Buuren, S.-J. Marrink, and H. J. C. Berendsen, J. Phys. Chem. **97**, 9206 (1993).
[12] F. F. Abraham, J. Chem. Phys. **68**, 3713 (1978).
[13] D. A. Rose and I. Benjamin, J. Chem. Phys. **100**, 3545 (1994).
[14] A. Chahid, F. J. Bermejo, M. Garcia-Hernandez, and J. M. Martinez, J. Phys. Condens. Matter **4**, 1213 (1992).
[15] K. M. Ewool and H. L. Strauss, J. Chem. Phys. **58**, 5835 (1973).
[16] V. Majer, L. Svab, and V. Svibida, J. Chem. Thermodyn. **12**, 843 (1980).
[17] M. Garcia-Hernandez, J. M. Martinez, F. J. Bermejo, A. Chahid, and E. Enciso, J. Chem. Phys. **96**, 8477 (1992).
[18] F. J. Bermejo, E. Enciso, J. Alonso, N. Garcia, and W. S. Howells, Mol. Phys. **64**, 1169 (1988).
[19] A. H. Narten, M. D. Danford, and H. A. Levy, J. Chem. Phys. **46**, 4875 (1967).
[20] L. J. Lowden and D. Chandler, J. Chem. Phys. **61**, 5228 (1974).
[21] I. R. McDonald, D. G. Bounds, and M. L. Klein, Mol. Phys. **45**, 521 (1982).
[22] S. E. DeBolt and P. A. Kollman, J. Am. Chem. Soc. **112**, 7515 (1990).
[23] F. S. Adan, A. Banon, and J. Santamaria, Chem. Phys. Lett. **107**, 475 (1984).
[24] E. M. Duffy, D. L. Severance, and W. L. Jorgensen, J. Am. Chem. Soc. **114**, 7535 (1992).
[25] P. Ahlström, A. Wallqvist, S. Engström, and B. Jönsson, Mol. Phys. **68**, 563 (1989).
[26] L. X. Dang, J. Chem. Phys. **97**, 2659 (1992).
[27] L. S. Bartell, L. O. Brockway, and R. H. Schwendeman, J. Chem. Phys. **23**, 1854 (1955).
[28] GAUSSIAN-92, Rev. A, M. J. Frisch, G. W. Trucks, M. Head-Gordon, P. M. W. Gill, M. W. Wong, J. B. Foresman, B. G. Johnson, H. B. Schlegel, M. A. Robb, E. S. Replogle, R. Gomperts, J. L. Andres, K. Raghavachari, J. S. Binkley, C. Gonzalez, R. L. Martin, D. J. Fox, D. J. Defrees, J. Baker, J. J. P. Stewart, and J. A. Pople (Gaussian Inc., Pittsburgh, 1992).
[29] J. Applequist, J. R. Carl, and K.-K. Fung, J. Am. Chem. Soc. **94**, 2952 (1972).
[30] K. L. Ramaswamy, Proc. Indian Acad. Sci. Sect. A **4**, 675 (1936).
[31] H. J. C. Berendsen, J. P. Postma, A. Di Nola, W. F. Van Gunsteren, and J.

R. Haak, J. Chem. Phys. **81**, 3684 (1984); J. P. Rykaert, G. Ciccotti, and H. J. C. Berendsen, J. Comput. Phys. **23**, 327 (1977).
[32] J. Miyazaki, J. A. Barker, and G. M. Pound, J. Chem. Phys. **64**, 3364 (1976).
[33] P. W. Atkins, *Physical Chemistry* (Oxford University Press, Oxford, 1982).
[34] A. H. Narten, J. Chem. Phys. **65**, 573 (1976).
[35] P. A. Egelstaff, D. I. Page, and J. G. Powels, Mol. Phys. **20**, 881 (1971).
[36] G. C. Lie, S. Grigoras, L. X. Dang, D.-Y. Yang, and A. D. McLean, J. Chem. Phys. **99**, 3933 (1993).
[37] S. Toxvaerd, Faraday Symp. Chem. Soc. **16**, 159 (1981).
[38] R. Evans, J. R. Henderson, D. C. Hoyle, A. O. Parry, and Z. A. Sabeur, Mol. Phys. **80**, 755 (1993).
[39] J. G. Kirkwood and F. P. Buff, J. Chem. Phys. **17**, 338 (1949).
[40] J. G. Harris, J. Phys. Chem. **96**, 5077 (1992).
[41] E. Salomons and M. Mareschal, J. Phys. Condens. Matter **3**, 3645 (1991).
[42] A. W. Adamson, *Physical Chemistry of Surfaces* (Wiley, New York, 1990).
[43] J. Chandrasekhar and W. L. Jorgensen, J. Chem. Phys. **77**, 5080 (1982); J. Chandrasekhar, W. L. Jorgensen, B. Bigot, and J. Chandrasekhar, J. Am. Chem. Soc. **104**, 4584 (1982).
[44] R. W. Imprey, M. Sprik, and M. L. Klein, J. Am. Chem. Soc. **109**, 5900 (1987).
[45] D. E. Smith and L. X. Dang, J. Chem. Phys. **101**, 7873 (1994).
[46] K. A. Peterson (unpublished).
[47] P. Bopp, in *The Physics and Chemistry of Aqueous Ionic Solutions*, edited by M. C. Bellissent-Funel and G. W. Neilson (Reidel, Dordrecht, 1987), p. 217.
[48] T.-M. Chang and L. X. Dang, J. Phys. Chem. (to be published).